Journal of Polymer Research (2022) 29: 357
https://doi.org/10.1007/s10965-022-03215-y

ORIGINAL PAPER

Extremely adherent and protective polymeric coating based on polydiphenylamine electrodeposited on steel in an organic electrolytic medium

Mimouna Bouabdallaoui[1] · Abdelqader El Guerraf[1] · Zaynab Aouzal[1] · Mohammed Bazzaoui[2] · Rongguang Wang[3] · El Arbi Bazzaoui[1]

Received: 14 April 2022 / Accepted: 27 July 2022 / Published online: 1 August 2022

Abstract
The present work fits into the efforts deployed to minimize the huge problems related to corrosion phenomena. As several industries are affected by the deterioration of metallic materials, new solutions need to be offered by the scientific community. In this context, we describe, in this paper, the electrochemical synthesis of polydiphenylamine coating (PDPA) on steel in an organic solution consisting of CH_2Cl_2 as solvent and $N(Bu)_4PF_6$ as supporting electrolyte. The electrolytic medium has been retained after a preliminary electrogravimetric study has shown that it can inhibit the working electrode dissolution without preventing the PDPA film formation. Spectroscopic and microscopic analyses were then achieved for the elaborated coatings. Analyses by X-ray photoelectron spectroscopy (XPS) and Fourier transform infrared spectroscopy (FTIR) have allowed a detailed characterization of the polymer (molecular structure, doping rate, chain length, …). In addition, morphological characterization by scanning electron microscope (SEM) confirmed that the value of the applied current density has a direct influence on the properties of the obtained polymer. The homogeneity and high adherence of the prepared PDPA film allow its use as a protective coating against steel dissolution. For this, corrosion tests were performed by studying the open-circuit potential (OCP), linear polarization curve (Tafel) as well as electrochemical impedance spectroscopy (EIS). The studies achieved in 3% NaCl solution have confirmed that the potential of the steel electrode shifts towards its passivation domain with the presence of PDPA coating. The latter is stable over time in contact with an aggressive solution and the inhibitory efficiency reached 97.2%.

Keywords Electrodeposition · Polydiphenylamine coating · Spectroscopic and microscopic characterization · Corrosion

Introduction

Among all metal alloys, steels stay the most frequently used materials. Though, their corrosion is the main problem and their protection is accomplished by numerous methods especially protective polymeric coatings. Indeed, conducting polymers such as polypyrrole [1–9], polyaniline [10–15] and polythiophene [16–19] have been widely used as anticorrosion coatings on several oxidizable metals. However, very limited number of papers have dealet with the case of polydiphenylamine (PDPA). All works carried out in this regard, focused on the polymerization processes and the properties of this polymer [20–24]. In addition, the electrodeposition of PDPA on oxidizable metals has never been reported and the most prepared coatings were obtained by chemical methods.

In this context, Nanocomposite coatings based on PDPA and vanadium pentoxide (V_2O_5) was used as a corrosion inhibitor for carbon steel. Corrosion resistance performance of these coatings in 5% NaCl solution was determined by electrochemical measurements and salt spray tests. Studies revealed very low j_{corr} (7.45 10^{-11} A.cm^{-2}), high E_{corr} (−0.04 V), impedance (1.69 10^{11} Ω.cm^2), and phase angle (84°) after 30 days exposure. An immersion test, in 1 M H_2SO_4

✉ Mimouna Bouabdallaoui
mimounabouabdallaoui@gmail.com

1 Laboratory of Applied Chemistry and Environment, Faculty of Sciences, Mohammed First University, Oujda 60000, Morocco

2 Materials and Environmental Laboratory, Faculty of Sciences, Ibn Zohr University, Agadir 80000, Morocco

3 Department of Mechanical Systems Engineering, Faculty of Engineering, Hiroshima Institute of Technology, 2-1-1 Miyake, Saeki-ku, Hiroshima 731-5193, Japan

solution for 24 h, was also achieved to examine the influence of corroding acid on the coatings [25].

Lingam [26] has synthesized Cu-PDPA nanocomposites by chemical polymerization of diphenylamine (DPA) followed by electrodeposition of copper in an acidified electrolytic bath. The Electrochemical impedance and Tafel polarization studies were performed for electrodeposited copper and Cu-PDPA nanocomposites in 3.5% NaCl solution. It has been shown that the Cu-PDPA nanocomposite coatings were more corrosion resistant than pure electrodeposited copper coating.

By a chemical process also, PDPA derivative was synthesized via diphenylamine, styrene, and formaldehyde. The anti-oxidative properties of the obtained PDPA were evaluated through oxidation–corrosion tests and differential scanning calorimetry [27].

In the same aim, DPA monomer was polymerized in the suspension of nano-crystalline SnO_2 to form inorganic–organic composite, in which SnO_2 was integrated within PDPA matrix/chain via *in-situ* oxidative polymerization. Electrochemical impedance spectroscopy (EIS) data substantiates the modified electrode affords higher electron transfer rate claims its diverse electro-analytical applications [28].

The objective of the present work is to improve the corrosion resistance of steel by means of adherent and homogeneous PDPA coating. The electrosynthesis of PDPA is carried out in dichloromethane in the presence of $N(Bu)_4PF_6$. The choice of this medium comes down to its synergistic effect in inhibiting the oxidation of the metal surface. The obtained films developed by different electrosynthesis techniques (potentiodynamic, galvanostatic and potentiostatic modes) have been characterized using various spectroscopic and microscopic analysis methods (FTIR, XPS, SEM). In addition, the behaviour of the prepared polymer on steel electrode toward an aggressive 3% NaCl solution was performed using linear polarization, electrochemical impedance spectroscopy and OCP methods.

Experimental

All chemicals were obtained from Sigma-Aldrich and were reagent grades so they were used as received.

The electrochemical experiments were performed in a one compartment cell using an Origalys potentiostat/galvanostat monitored by Origamaster 5 software. As evidenced by XPS measurements, the working electrode was a Steel disk with a chemical composition of 58.5% Fe, 18.3% O, 8.9% C, 7.4% Mn, 2.4% Si and other element traces (Fig. 1). The auxiliary electrode was a platinum plate, and all potentials were measured vs. a saturated Ag/AgCl reference electrode.

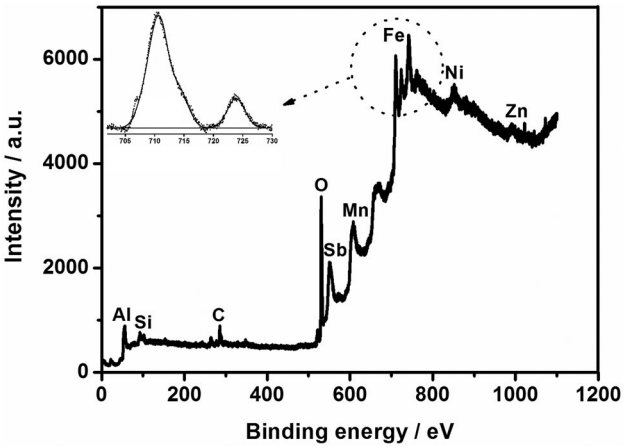

Fig. 1 XPS spectrum showing the chemical composition of the working electrode

The adherence tests were performed via the standard Sellotape test TESA-4204 BDF tape. Polymeric films were cut into small squares, the adhesive tape is fixed on the surface of the coating and then stripping it. The ratio between the number of adherent film squares remaining and their total number gives the adherence percentage.

X-ray photoelectron spectroscopy analysis was performed with a Vacuum Generators Escalab MKI spectrometer equipped with Mg Kα (1256.6 eV) and Al Kα (1486.6 eV) sources operating at 200 mW. The Spectra were calibrated against the 1 s carbon electron peak (285 eV binding energy) of the polydiphenylamine ring carbon atoms as internal reference. The scanning electron micrographs of all samples were taken using JOEL Ltd., JXA-8900 instrument. Fourier transform infrared spectrometry analysis was carried out using a JASCO FT/IR-4200 spectrophotometer.

The conductivity measurements were performed using a home-made equipment and wherein the polymer is sandwiched between the metallic electrode and a mercury contact (Fig. 2). Its impedance (R) is then measured and its conductivity deduced following equation:

$$\chi = \frac{1}{R}\frac{e}{S}$$

where R is the electrical resistance; χ is the conductivity; e: the thickness of the coating and S represent the surface of the polymeric film which is in contact with the mercury layer.

The electrochemical impedance spectroscopy measurements were performed at an open circuit potential with a 10 mV as amplitude of the superimposed AC signal, and the applied frequency ranged from 1 kHz to 10 mHz. The fitting of the recorded EIS curve was achieved using Zsimpwin software. All electrochemical corrosion

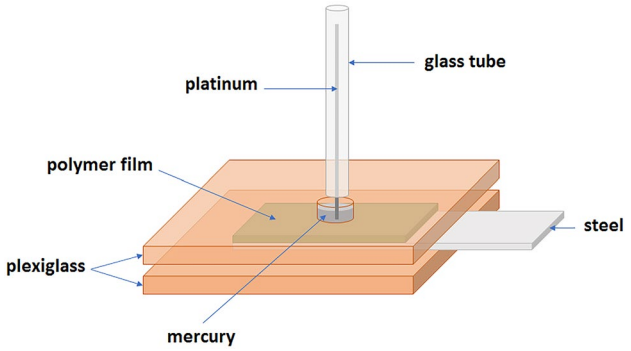

Fig. 2 Device developed in the laboratory and used for conductivity measurements

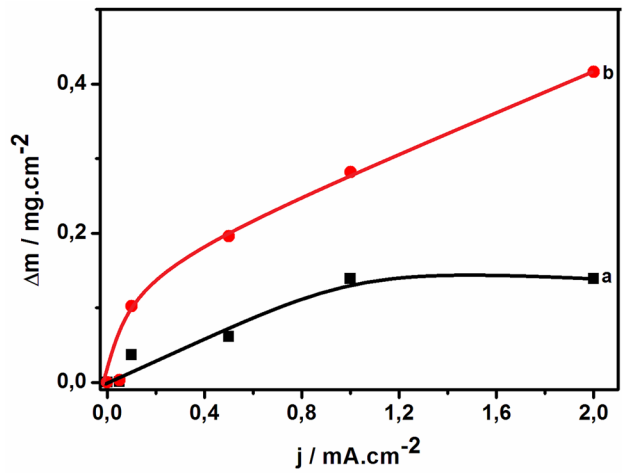

Fig. 3 Electrogravimetric curves recorded on steel in the absence (**a**) and in the presence (**b**) of the DPA monomer

measurements were performed at room temperature in 3% NaCl solution.

Results and discussion

Electrosynthesis of PDPA on steel electrodes

Electropolymerization can be performed by several electrochemical techniques. These techniques have a great influence on the electropolymerization reaction and on the "quality" of the obtained polymer (morphology, homogeneity and adherence). Thus, in this section, we will examine the effect of the potentiodynamic and galvanostatic methods on the electropolymerization of DPA.

The potentiodynamic mode makes it possible to follow the steps of the electropolymerization process to identify the oxidation potential of the monomer and the oxidation and reduction peaks of the polymer. Beforehand, the behaviour of the working electrode in the absence of the DPA is mandatory as it helps to differentiate the peaks of the metal and the electrolytic medium from those of the polymer. For this, we have also studied the electropolymerization process on a noble metal, platinum (Pt), for comparison.

Before starting the electropolymerization, we evaluate the inhibitory effect of the electrolytic medium (CH_2Cl_2 + $N(Bu)_4PF_6$) on the dissolution reaction of the working electrode, which favors the electropolymerization reaction of DPA. The study is carried out by electrogravimetry, in the absence and in the presence of the monomer. It involves imposing current densities to the working electrode for a period of time and measuring the resulting change in mass Δm. The value and the sign of Δm provide information on the electrochemical behaviour of the electrode.

The electrolytic medium, particularly the supporting electrolyte, plays a key role in the electrodeposition of conducting polymers (CPs) on oxidizable metals. Indeed, the used salt must be chosen so that it promotes the passivation of the working electrode.

Tetrabutylammonium hexafluorophosphate $N(Bu)_4PF_6$ is known by its passivation effect [29–33]. An electrogravimetric study on the effect of salt on the electropolymerization of thiophene confirmed that, among several used salts, the best results are obtained in the case of $N(Bu)_4PF_6$ with a faradic yield of 85% [34]. For these reasons we have chosen this supporting salt to study the electropolymerization of DPA in organic medium.

A series of steel electrodes, whose chemical compositions are described in the experimental part (Fig. 1), have been polished, rinsed, dried and weighed. Current densities ranging between 0.05 and 2 $mA.cm^{-2}$ were applied to the working electrode for 5 min in CH_2Cl_2 + 0.1 M $N(Bu)_4PF_6$ electrolytic medium.

In the absence of the DPA monomer, according to the electrogravimetric curves (Fig. 3), a slight positive variation of the mass is observed. This change as a function of the imposed current density rapidly evolves towards a plateau when j exceeds a few tenths of $mA.cm^{-2}$. This indicates the formation of a passivation layer based on oxides and fluorinated compounds on the surface of the electrodes, resulting from the decomposition of the salt, by analogy with the work carried out on AsF_6^- [35] and in agreement with the explanations of literature [34]:

$$PF_6^- \rightleftharpoons PF_5 + F^-$$

In turn, PF_5 can be reduced according to the reaction:

$$PF_5 + 2\,e^- \rightleftharpoons PF_3 + 2\,F^-$$

Overall, the decomposition of the counterion is described by the following reaction:

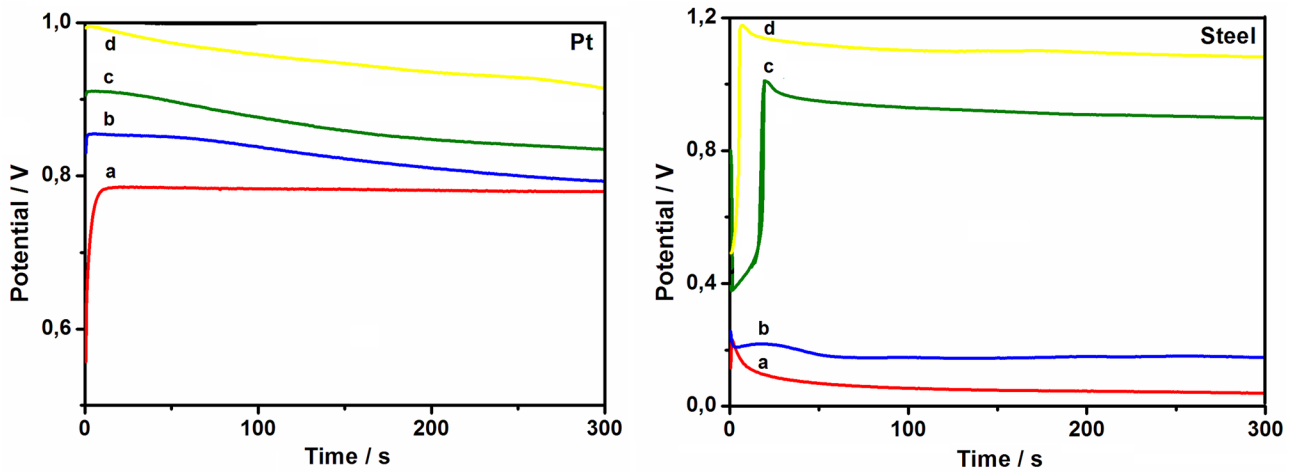

Fig. 4 Chronopotentiometric curves recorded on platinum and steel in (CH_2Cl_2 + 0.1 M $N(Bu)_4PF_6$ + 0.5 M DPA) medium. Applied current densities: **a** 0.1; **b** 0.5; **c** 1; **d** 2 mA.cm^{-2}

$$PF_6^- + 2\,e^- \rightleftharpoons PF_3 + 3\,F^-$$

The fluoride ions F^- resulting from the decomposition of PF_6^- are the origin of the passivation of the metal.

When the monomer is added to the electrolytic medium, Δm increases rapidly, indicating the formation of the polymer on the surface of the electrode.

Chronopotentiometric curves recorded on platinum and steel are shown in Fig. 4. The curves vary according to the nature of the metal and the applied current density.

In the case of platinum, for a relatively low current density j = 0.1 mA.cm^{-2}, the polymerization does not start. The formation of the polymer is only observed at 0.5 mA.cm^{-2}. By increasing the current density to 1 mA.cm^{-2} a thin and inhomogeneous green film is obtained. Beyond this value, the films are black, thicker and homogeneous.

In the case of steel, the polymerization is initiated at higher current densities because of the metal dissolution reactions that compete with the electropolymerization reaction. At current densities j < 0.5 mA.cm^{-2} potential stabilizes at 0.2 V (Table 1). This low value is below the oxidation threshold of the monomer; therefore, nothing is formed on the surface of the electrode. By applying 1 mA.cm^{-2}, the potential increases to 0.92 V and a very thin green film with edge effects is deposited on the surface of the electrode after a preliminary stage of germination during which a competition with the dissolution of the metal is established and lasts a few seconds. A thick, black and homogeneous film is obtained from 2 mA.cm^{-2}.

Assuming that the mass variation is entirely due to the formation of the polymer, the value of the faradic yield of the electropolymerization reaction can be deduced by taking the imposed current density j = 2 mA.cm^{-2} by the formula:

$$Y = m_{exp}/m_{th} \text{ with } m_{th} = \left[\left(M_M + yM_A\right)Q\right]/\left[(2+y)F\right]$$

M_M: molar mass of the monomer
M_A: molar mass of the doping anion
y: doping rate
Q: applied load
F: Faraday

Assuming sufficiently important chain lengths and a 50% doping rate, the polymerization requires 2.5 electrons per monomer. These hypotheses make it possible to calculate a theoretical mass of polymer per charge consumed, if all the oligomers are deposited on the substrate. The polymerization yield can then be estimated by calculating

Table 1 Electropolymerization of DPA in organic medium on Pt and steel by the galvanostatic mode

	Pt			Steel		
j (mA.cm^{-2})	E (V)	Formation	Homogeneity	E (V)	Formation	Homogeneity
0.1	0.78	-		0.1	-	
0.5	0.81	+	-	0.2	-	
1	0.85	+	-	0.92	+	-
2	0.93	+	+	1.5	+	+

+,- PDPA film obtained or not, homogeneity good or bad

the ratio of the experimental mass to the theoretical mass according to the above formula. Thus, for a charge density of 0.6 C.cm^{-2} (2 mA.cm^{-2} for 5 min), the yield is of the order of 69%.

This preliminary study showed that the electrolytic medium consisting of CH_2Cl_2 as solvent and $N(Bu)_4PF_6$ as salt allowed the inhibition of the dissolution of the working electrode and the growth of a PDPA film. In what follows, we have used this medium to study the electropolymerization reaction of DPA by potentiodynamic technique.

Figure 5 represents the voltammograms recorded on platinum and steel in the absence (A) and in the presence (B) of DPA. On Pt an oxidation peak at 0.9 V is observed in the absence the of the monomer, which can be attributed to the oxidation of PF_6^- by analogy with observations reported in the literature [34]. The voltammogram recorded on steel is complex with several redox peaks. The first scan shows three oxidation peaks, the one at 0.9 V can be attributed to the oxidation of PF_6^- [34] and the others could be due to oxidation of the substrate. The current decreases from 2 to 1.2 mA.cm^{-2} after the first three scans.

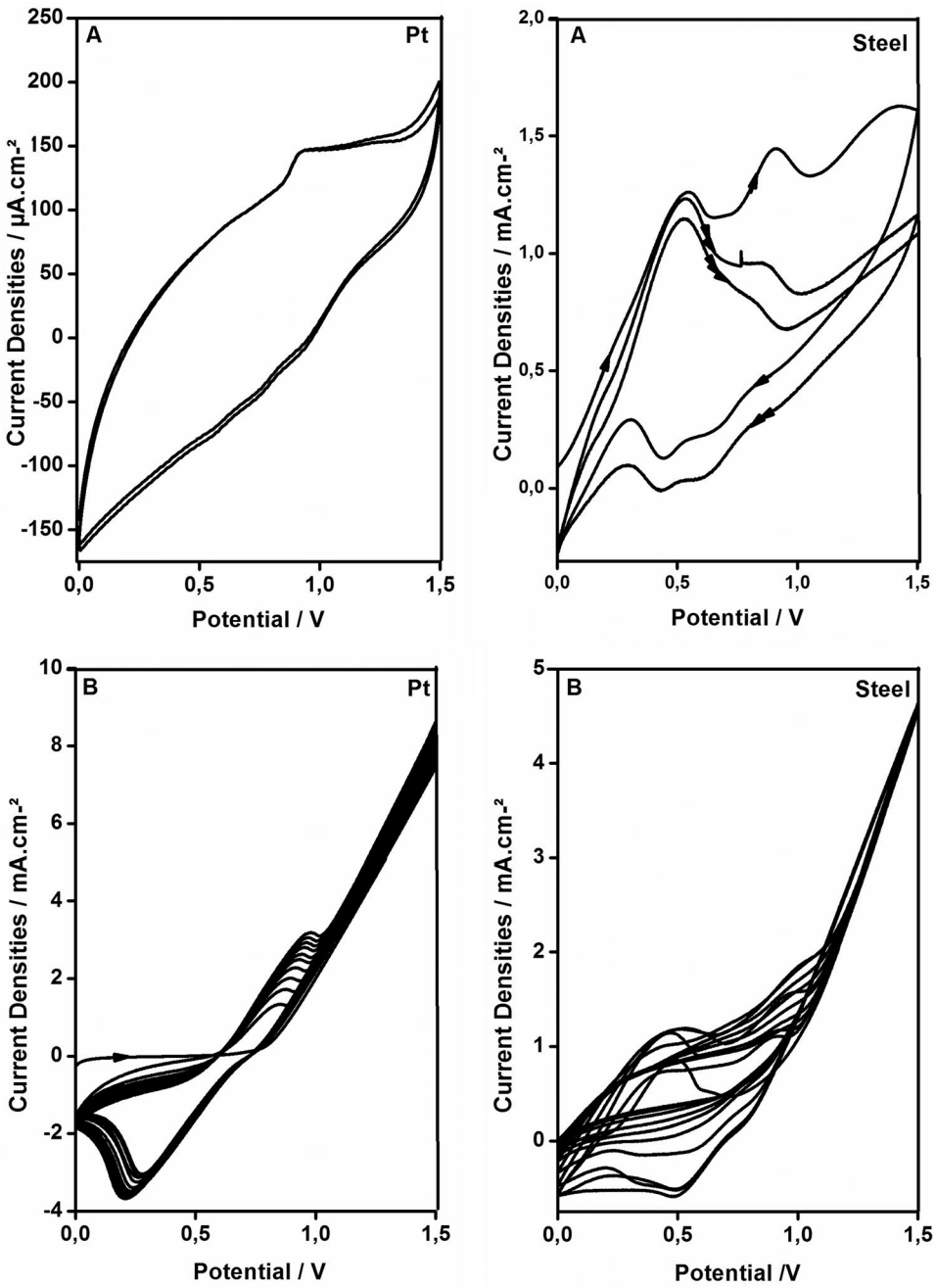

Fig. 5 Voltammograms recorded on platinum and steel in the absence (**A**) and in the presence (**B**) of DPA. scan rate 100 mV.s^{-1}

After the addition of the 0.5 M DPA to the electrolytic medium (0.1 M CH_2Cl_2 + $N(Bu)_4PF_6$), the curves show increasing trends on both metals. On Pt, the oxidation wall of the monomer is identified at 0.8 V and a couple of redox peaks of the polymer at (0.85 V oxidation, 0.22 V reduction) are well observed. A blackish-green PDPA film is formed on the surface of the electrode.

In the case of steel, the voltammograms show varied and complex shapes. A competition is established between the electropolymerization reaction and the oxidation of the metal. Here, the active dissolution of the metal substrate predominates and inhomogeneous films are formed on the surface of the working electrode. It should be noted that a deposit is obtained only on the edges of the metal due to the fact that the density of the current is greater; this phenomenon is known as the edge effect.

After the electrosynthesis step, the PDPA films were characterized by various analytical techniques in order to access the structure, the elemental composition and the morphology of the coatings.

Characterization of PDPA films

Firstly, PDPA Electrodeposited on steel by galvanostatic mode was analyzed by XPS. The carbon, nitrogen, phosphorus and fluorine signals were decomposed and the ratios of the intensities of the different components were calculated to access the elemental composition of the polymer backbone and its doping level.

Figure 6 shows the C1s and N1s XPS signals of the doped and undoped PDPA films. Deconvolution of the C1s carbon signal revealed the presence of five peaks. The intense peak taken as a reference at 285 eV corresponds to the carbon of the C–C and C-H bonds [36, 37]. The peak at 287.1 eV can be attributed to groups C-N and C = N [38, 39]. The peak at 289 eV corresponds to C-N^+ and C = N^+ [40]. The intensity

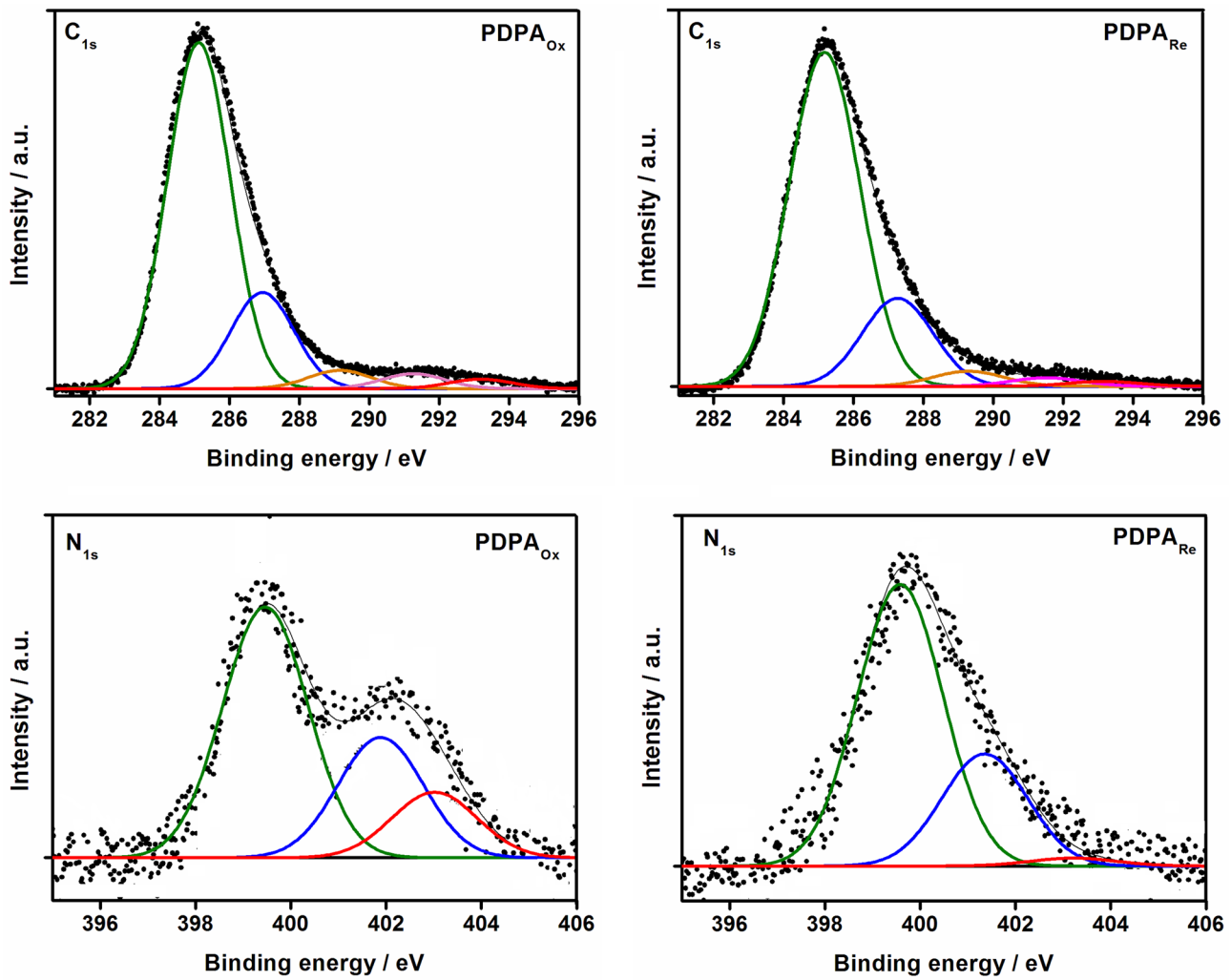

Fig. 6 Decomposition of the C1s and N1s XPS signals of doped and undoped PDPA films synthesized by the galvanostatic mode on steel in (CH_2Cl_2 + $N(Bu)_4PF_6$ 0.1 M + DPA 0.5 M) electrolytic medium

of this peak drops after dedopage of the PDPA films with ammonia (Table 2), which confirms the hypothesis that this component is due to an interaction between the carbon skeleton of the polymer and the doping anion. The peaks at 291.4 and 293.2 eV are attributed to groups C–OH and C = O respectively [36–40]. They may be originating from carbon contamination or likely over-oxidation which leads to oxygen groups fixed on the chains of the polymer [16, 41].

The nitrogen signal consists of three components. The first at 399.3 eV corresponds to nitrogen doubly bound to carbon C = N. The second component at 401.8 eV is attributed to nitrogen from the C-N group. The last peak at 403 eV corresponds to nitrogen atoms carrying a positive partial charge ($C = N^+$ and $C\text{-}N^+$). The relative intensities of these components decrease as the degree of oxidation of the polymer decreases.

The ratios of the total carbon signal to the nitrogen signal range from 14 to 17 depending on the oxidation state of the polymer. These values are close to the theoretical value of 12 (12 carbons for each nitrogen). The difference comes from the presence of carbon atoms of contamination.

The fluorine signal can be decomposed into two components at 686 and 687.2 eV from the PF_6^- counter ion of the electrolyte salt (Fig. 7). The first component at 686 eV corresponds to the fluorine of the PF_6^- [42, 43] doping anion. The second component at 687.2 eV could be due to the formation of C-F bonds during the electropolymerization, resulting from the decomposition of the salt ($PF_6^- + 2\,e^- \rightleftharpoons PF_3 + 3\,F^-$) [44, 45]. Doping rate calculated by total fluoride to total carbon intensity ratios is 43%.

The phosphorus signal in the oxidized PDPA sample has a single doublet at (135.2, 136.7 eV). The doublet corresponds to the phosphorus atoms of the PF_6^- [46, 47] doping anion. In the reduced films no phosphorus signal is detected, which reflects that the polymer is completely undoped after treatment with ammonia.

To confirm the results obtained by XPS, particularly those concerning the doping-undoping of the polymer, oxidized and reduced samples were analyzed by FTIR spectroscopy. Figure 8 shows the FTIR spectra of the films deposited on steel by galvanostatic mode. Both spectra have substantially the same appearance and consist of the same bands. The first remark concerns the "quality" of the spectra: that of the reduced form of the PDPA have a high signal/noise ratio, the bands are thin and better resolved than that belonging to the spectra of the oxidized state. This observation is related to the degree of order in the polymer chains and which is more important in the case of undoped reduced films. Indeed, it is well known that when the film is oxidized, there is the insertion of counter-ions from the electrolytic medium to compensate the excess of positive charges on the backbone of the polymer. Thus, under the effect of stearic hindrance the chains are distorted. Added to this is the creation of side groups attached to the polymer, which increases the rate of structural defects and decreases the length of conjugation. This behaviour during the doping-undoping process has been studied in detail by resonance Raman spectroscopy (RRS) and surface-enhanced Raman spectroscopy (SERS) in the case of other conductive polymers [48–52].

Bands at 1600 and 1500 cm^{-1} correspond to the C = C bonds elongation of the benzene rings [53, 54]. The absorption band at 1490 cm^{-1} comes from the vibrations of the N–H bond (shears) and the bands between 1240 and 1350 cm^{-1} are due to shear vibrations C-N [55, 56]. The low intensity bands at 696 and 750 cm^{-1} correspond to off-plane vibrations of the C-H bonds of the monosubstituted phenyls [57, 58]. The intensity of these bands is considerably high in the monomer spectrum presented by Athawale et al. [21]. The band around 800 cm^{-1} is due to the vibration of the C-H para-disubstituted phenyls [59, 60], it is absent in the spectrum of the monomer [21]. Athawale et al. [21] have noticed that the band at 1490 cm^{-1} (N–H) is light in comparison with that observed on the monomer spectrum, for this reason they assumed that the coupling is also via the amine group.

The C-H vibration bands of the phenyls make it possible to approach the chain length of the synthesized polymers. Indeed, if it is supposed that the polymerization is carried out solely by C–C coupling, it is possible, by calculating the ratio of the intensities of the bands corresponding to the monosubstituted and para-disubstituted phenyls, to deduce therefrom the average mass of the polymer. This method was applied to the ratio of the bands at 696 and 800 cm^{-1} then with the bands at 750 and 800 cm^{-1} and chain lengths between 50 and 100 are obtained.

The C-N vibration bands at 1240 and 1350 cm^{-1} and the N–H shear vibration band at 1490 cm^{-1} provide a qualitative assessment of the doping rate of PDPA films. Indeed, the absorption bands at 1240 and 1490 cm^{-1} correspond to

Table 2 Intensity ratios of the different components of the XPS signals for oxidized and reduced PDPA films

Sample	Intensity ratios (%)										
	C_i/C_{total}					N_i/N_{total}			F_i/F_{total}		P_i/P_{total}
	C_{285}	$C_{287.1}$	C_{289}	$C_{291.4}$	$C_{293.2}$	$N_{399.3}$	$N_{401.8}$	N_{403}	F_{686}	$F_{687.2}$	$P_{doublet}$
$PDPA_{Ox}$	76	16	4.4	2.1	1.5	55.7	28	16.3	86.8	13.2	~100
$PDPA_{Re}$	82.5	12.1	3.8	0.7	0.9	62.6	32.4	5	57.6	42.4	~0

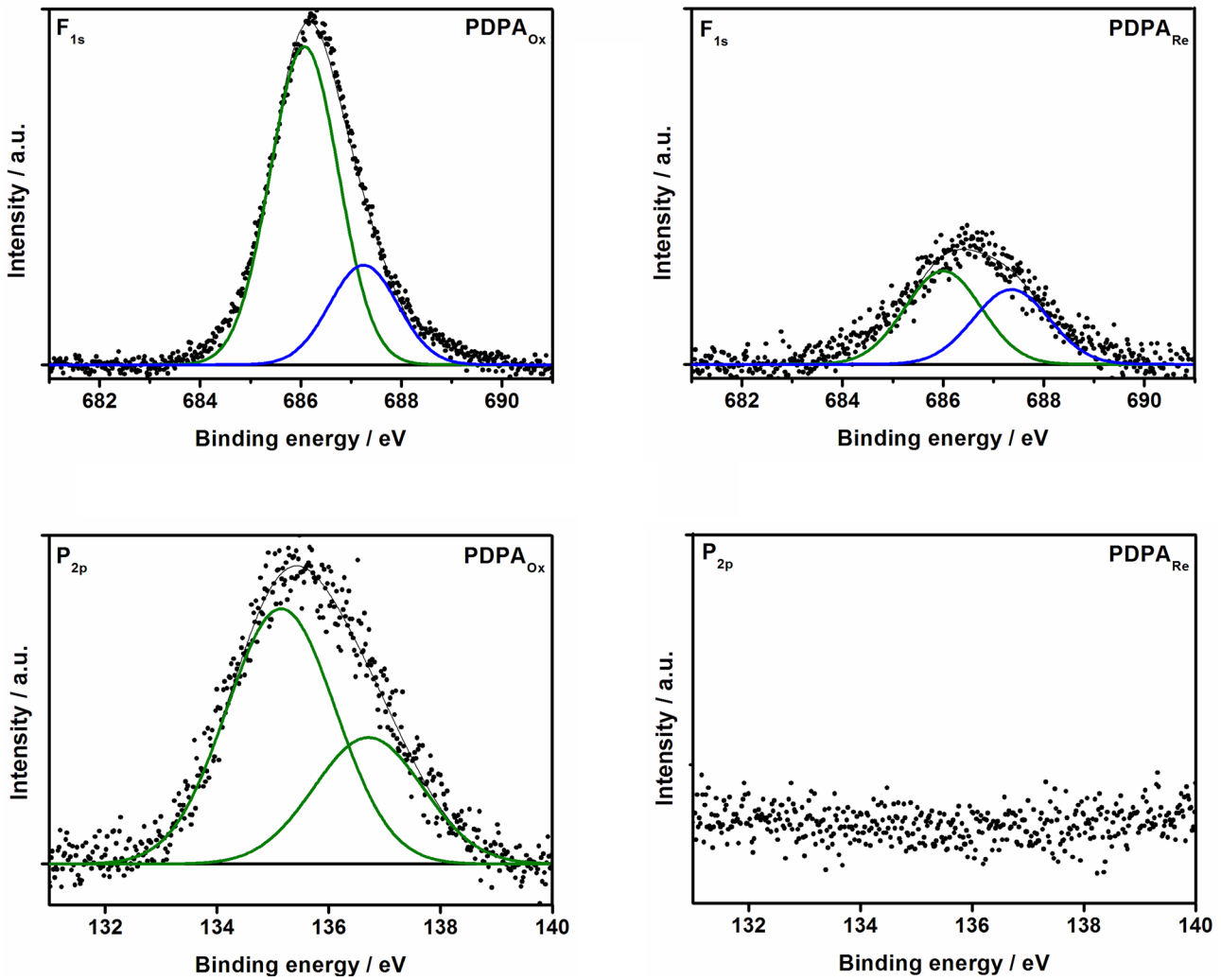

Fig. 7 Decomposition of the F1s and P2p XPS signals of doped and undoped PDPA films synthesized by the galvanostatic mode on steel in (CH_2Cl_2 + $N(Bu)_4PF_6$ 0.1 M + DPA 0.5 M) electrolytic medium

the phenylamine form of PDPA and the band at 1350 cm^{-1} refers to the quinone-imine form.

Bands at 550; 845 and 1155 cm^{-1} are characteristic of the oxidized form; they are of low intensities or completely absent in the reduced form. These bands could come from modes of vibration of the doping anion or result from interactions with PF_6^- [61, 62].

The adherence of the same samples, estimated by the standard Sellotape test, given in %, was good. The polymer is extremely adherent (100%).

The conductivity measurements were also achieved on reduced and oxidized PDPA films synthesized by galvanostatic mode on steel electrodes. The results of the measurements are collated in Table 3. The thicknesses of the films are estimated by scanning electron microscopy (SEM). As expected, the conductivity of the oxidized film is greater than those of the reduced film. The conductivity of oxidized films is 0.31 10^{-3} $S.cm^{-1}$. For reduced film, the conductivity value is very low 0.35 10^{-11} $S.cm^{-1}$, reflecting the insulating nature of the reduced PDPA.

Generally, conjugated polymers are conductive in the doped form and insulating in the undoped neutral state. Conductivity develops during doping process of the polymer. Polymeric chains in a film are negatively charged in the case of reduction and positively charged in the case of oxidation. To maintain electroneutrality, counterions diffuse into the film during charging and out of the polymer during discharging. These phenomena are explained by the bipolaron model [63]. Bipolarons are equivalent to diionic states of a system after oxidation or reduction from the neutral state. The transition from the neutral state to the bipolaron takes place via the polaron state, monoion. Additional local distortions occur in the chain during the charging of the polymer.

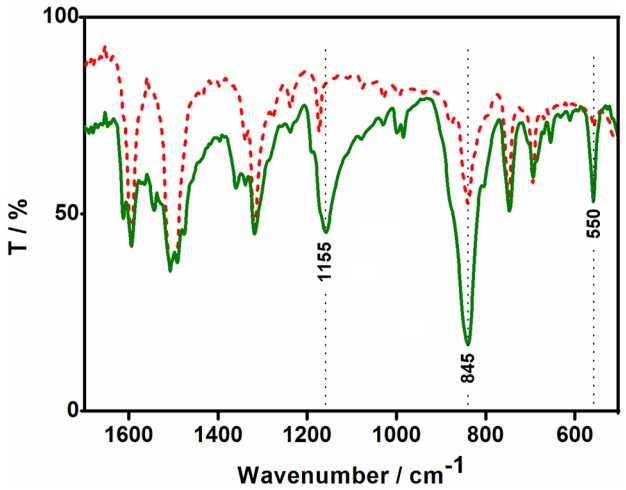

Fig. 8 FTIR spectra of oxidized (—) and reduced (-----) PDPA films, electrodeposited on steel by the galvanostatic mode

The mechanism of charge transport in electroactive polymers is based on electron hopping between oxidized and reduced sites of a redox state [63]. The bipolaron model has supposed that charge transport occurs along single infinite long chains. However, the knowledge that the chain lengths of conjugated polymers are relatively short, ranging on average between 30 and 60 units, has led to the conclusion that the ratedetermining transport step is intermolecular and should be described by a hopping process.

The maximum conductivity should be observed when the amount of oxidized and reduced sites of a redox state is equal. By contrast, conductivity measurements of conjugated polymers reveal that maximum conductivity arises at high doping, indicating that the charge carriers in that regime are spinless [63]. Spinless bipolarons could become mobile at high dopant concentrations, where the Coulomb attraction with counterions is largely screened. At very high charging levels, the bipolaron model predicts that the broadening of the bipolaron states in the gap leads to the merging of the lower and upper bipolaron bands with the valence band (VB) and the conduction band (CB), respectively. This effect produces a new unfilled VB band and, therefore, a transition to metallic-like transport properties.

From the viewpoint of physicists, conducting polymers may be considered as strongly disordered semiconducting materials [63]. Their transport properties can be described by the variable-range hopping model (VRH), where conduction occurs by hopping between electronically localized states in the band gap.

Table 3 Conductivities of reduced and oxidized PDPA films electrodeposited on steel electrodes by the galvanostatic mode

Film	S (cm^2)	e (µm)	R (Ω)	χ ($S.cm^{-1}$)
$PDPA_{Ox}$	0.38	7	5.821	$0.31\ 10^{-3}$
$PDPA_{Re}$			$473\ 10^4$	$0.35\ 10^{-11}$

The morphology of the samples was then analyzed by SEM (Fig. 9). The films have different topography depending on the applied current density and the electrosynthesis time. Indeed, the film synthesized at a current density of 1 $mA.cm^{-2}$ for 10 min, corresponding to a charge density of 0.6 $C.cm^{-2}$, has a random lamellar structure. The lamellae have different sizes and do not seem to have a privileged orientation, but overlap to form an amorphous network. As soon as the electrical charge of electrosynthesis is increased ($Q = 2.7\ C.cm^{-2}$), the morphology changes.

Properties of polymers depend on the electropolymerization method. In addition, experimental parameters like electrical charge of electrosynthesis are also important for the quality and the properties of the polymer. In particular, the formation current in a galvanostatic experiment determines the chain length and structure of the film [63]. Very high currents, which imply the formation of highly charged and reactive intermediates, lead to defects and the formation of cross-linked materials. At low electrical charges, the oligomeric intermediates are weakly charged, and consequently, the electropolymerization may end at an oligomeric level.

Electropolymerization starts with the formation of oligomers in solution. The next step is the deposition, which includes nucleation, growth, and additional chemical steps under solid-state conditions. There are two types of nucleation, namely instantaneous and progressive, and three types of growth involving one- (1D), two- (2D), and three-dimensional (3D) processes. In the instantaneous nucleation, the number of nuclei is constant and they grow without the formation of further nuclei. In the case of progressive nucleation, nuclei are generated at all times. 1D growth takes place only in one direction, e.g. perpendicular to the electrode. In the 2D growth, the nuclei grow parallel to the electrode, and in the 3D growth, the rates for these processes perpendicular and parallel to the electrode are very similar.

In addition, the polymer formation and its oxidation (doping) occur simultaneously. Every third to fourth monomeric subunit will be charged at the end of the electropolymerization [63].

The charge Q is related to the polymer thickness δ by the equation [64]: $\delta = \frac{QM}{0.5FA\rho}$, where M and ρ are the molecular weight and the density of the monomer respectively, A is the area of the electrode and F the Faraday's constant.

Corrosion tests

Among the potential applications of the new coating, its use as a physical barrier against corrosion phenomenon. We have therefore undertaken an electrochemical study to evaluate

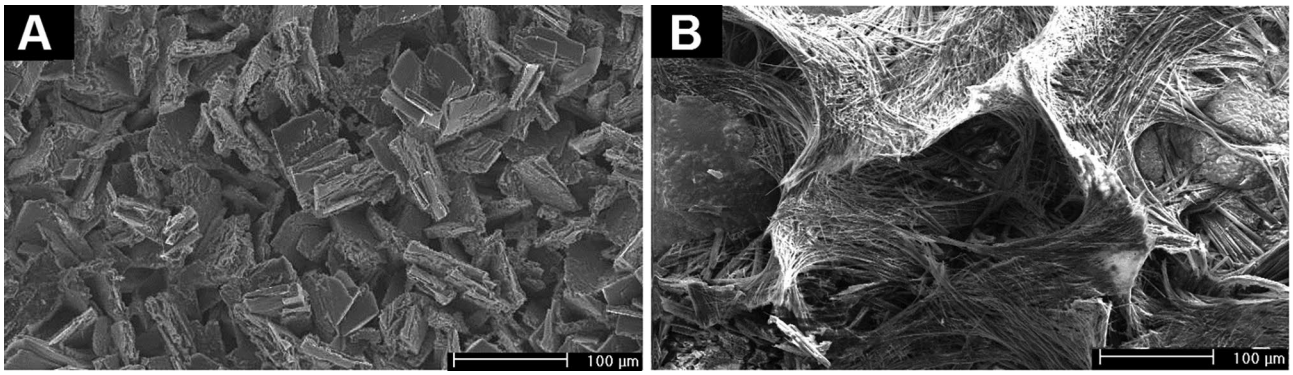

Fig. 9 SEM micrographs of PDPA deposited on steel. **A** Q = 0.6 C.cm^{-2}. **B** Q = 2.7 C.cm^{-2}

the protection performance of electrodeposited PDPA on steel. The study was conducted by three techniques: i) open-circuit potential (OCP) measurement, ii) determination of corrosion current density based on linear polarization curve (Tafel method) and iii) electrochemical impedance spectroscopy (EIS).

The first method provides information on the behaviour of the metal. The measurement of the open circuit potential E_{OC} over time makes it possible to follow the evolution of the behaviour of the polymer/metal system immersed in a corrosive electrolytic solution. The experiments were undergone for144 h immersion time in an aggressive solution of 3% NaCl and allowed to evaluate the stability of the polymeric coatings (Fig. 10A). The coating/metal system goes through two stages. At the beginning of immersion, a first transitional stage, which lasts for 50 h, results in the reduction of the potential. The drop in EOC is explained by an interaction between the coating/metal and its environment which leads to transformations, exchange and maybe a slight degradation of the PDPA/metal system. Followed by a period of stability where the system adapts to the surrounding conditions and the transformations and exchange decrease. The initial potential (at t_0 = 0 h) of the coated metal is shifted to a more anodic value (-569 mV) than the potential of uncoated electrode (-608 mV). This shows that the PDPA film moves the potential of the steel electrode towards its passivation range. During the immersion, we recorded a decrease in abandonment potential during the 48 h at a potential of -686 mV. After 48 h the potential stabilizes. The solution becomes yellow and a precipitate due to the oxidation of the metal surface under the effect of chloride ions is formed at the bottom of the cell after 72 h. In the case of bare steel, the yellow precipitate forms immediately after immersion in saline medium. The film does not come off the surface of the metal, but the corrosion products diffuse to the solution through the polymer. This steel behaviour is usual in aggressive environments. The dissolution reaction of the steel in an aqueous medium is:

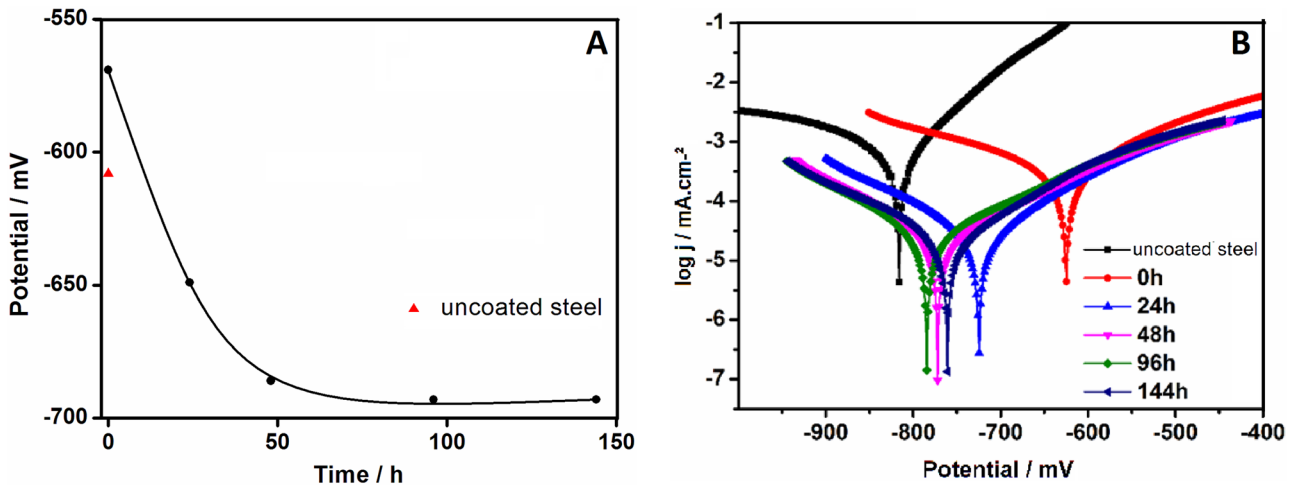

Fig. 10 Electrochemical study of PDPA-coated steel electrode in an aggressive solution of 3% NaCl at different immersion times. **A** Evolution of the open-circuit potential. **B** log[j] = f(E) Tafel curves

$$Fe \rightarrow Fe^{2+} + 2\,e^{-}$$

Reduction of the corrosive agent:

$$O_2 + 2\,H_2O + 4\,e^{-} \rightarrow 4\,OH^{-}$$

The corrosion product:

$$Fe^{2+} + 2\,OH^{-} \rightarrow Fe(OH)_2$$

This ferrous hydroxide $Fe(OH)_2$ or hydrated ferrous oxide ($FeO.nH_2O$) constitutes a greenish-black layer on the surface. In the presence of oxygen, Fe^{2+} is oxidized to Fe^{3+}. Ordinary rust is the product of this step:

$$4\,Fe(OH)_2 + O_2 + 2\,H_2O \rightarrow 4\,Fe(OH)_3$$

The hydrated ferric oxide has an orange to red-brown colour. It exists in the form of non-magnetic Fe_2O_3 (haematite) or magnetic $Fe_2O_3.Fe_3O_4.nH_2O$ [65]. Thus, rust films can contain up to three layers of iron oxides in different oxidation states [66].

The corrosive agent infiltrates through the film on the surface of the metal. An amount of the metal hydroxide that forms on the surface of the steel turns into iron oxide because of its low solubility product, thus forming a passive film which protects the metal from corrosion according to the reactions described above:

$$Fe(OH)_2 \rightarrow FeO + H_2O \text{ and } 2\,Fe(OH)_3 \rightarrow Fe_2O_3 + 3\,H_2O$$

In this context, a study of the variation of open circuit potential over time for a vinyl coating containing 0 to 5% of PDPA deposited on steel was conducted by Sathiyanarayanan et al. [67]. The authors found that the potential of coated plates containing PDPA (3% and 5%) increases after 80 days of immersion compared to the coating that does not contain PDPA. They proposed a steel protection mechanism by the PDPA similar to that of polyaniline, based on the oxidation–reduction potentials of the polymers that are neighbours. They bound the passivation of the metal to the oxidoreduction capacity of the polymer.

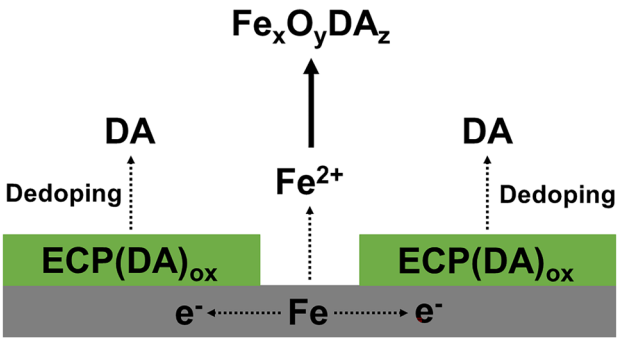

Fig. 12 Proposed corrosion protection mechanism according to Minh and Quoc [65]. ECP: electronic conducting polymer; DA: doping anion

Beck et al. [68] suggested a two-step mechanism: i) dedoping (reduction of the film) which is counterbalanced by an anodic overoxidation reaction and ii) the chemical attack of nucleophiles of the radical-cations (Fig. 11). The reactants H_2O, OH^- and A^- do not react only to the surface, but infiltrate into the conductive polymer film. In the case of polypyrrole, anodic overoxidation provides the anodic process [69]. The conjugation is interrupted. However, in the case of polythiophene, the overoxidation is concentrated on the S atom, leading to a sulfone group. Therefore, the conjugation is not interrupted.

Minh and Quoc [65] assume that dopant anions DAs form insoluble complexes with iron ions $Fe_xO_yDA_z$ and can prevent further corrosion (Fig. 12). The use of big anions such as polystyrenesulphonate and dodecyl sulphate could improve corrosion protection by preventing the entry of chloride [70].

To confirm the results obtained by monitoring the free potential, we performed a linear polarization study of the samples at different open-circuit immersion times in 3% NaCl (Fig. 10B). The potentials and the corrosion currents are determined from the Tafel lines by extrapolation of the parts corresponding to the strong polarizations of the log|j| = f(E) curves. The inhibitory efficiency E (%) is obtained

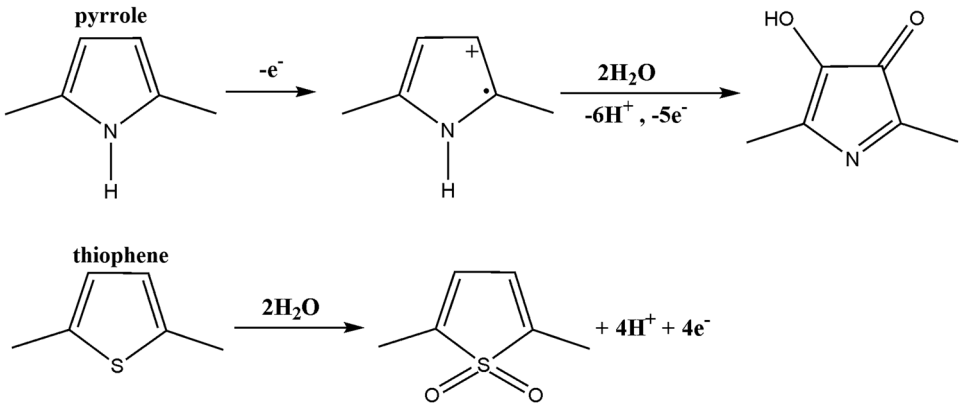

Fig. 11 Anodic overoxidation reaction and chemical nucleophilic attack in the case of polypyrrole and polythiophene [68]

Table 4 Corrosion parameters: corrosion potential (E_{corr}), corrosion current density (j_{corr}) and inhibitory efficiency (E (%)) of the PDPA-coated steel at different immersion times

t (h)	E_{Corr} (mV)	j_{Corr} (μAcm^{-2})	E (%)
Bare metal	-821	1.78	-
0	-625	0.63	64.6
24	-723	0.08	95.5
48	-773.9	0.06	96.6
96	-781.5	0.04	97.7
144	-763.1	0.05	97.2

by the equation: $E(\%) = (j^0_{corr} - j_{corr})/j_{corr}$; where j^0_{corr} and j_{corr} are corrosion current densities of bare metal and PDPA coated metal respectively. Corrosion parameters (E_{corr}, j_{corr} and E (%)) are summarized in Table 4.

The potential and the corrosion current decrease slightly during immersion. These results are consistent with the evolution of open circuit potential. The values of the current densities are comparable and coherent. The stability of the currents reflects the stability of the PDPA/Steel system in the corrosive medium which indicates a corrosion inhibition effect. The inhibitory efficiency increases from 64.6% at the beginning of immersion to 95.5% after 24 h and reaches 97.2% at the end of immersion. These results were expected given the results of the adherence tests.

The corrosion resistance of electrodeposited PDPA coatings was also studied by electrochemical impedance spectroscopy (EIS). Impedance spectroscopy can reveal interfacial changes due to the modification of the surface of the electrode. Figure 13A shows the electrochemical impedance loops measured at the abandonment potential. The impedance diagram makes it possible to study the evolution of the system through the values of each parameter defined by the electrochemical impedance diagram. The analysis of the evolution of the values of these parameters informs on the evolution mechanism of the coated metals: penetration of the electrolyte in the coating, corrosion of the metal, detachment of the film…

The impedance diagrams have a single capacitive/inductive loop through the different immersion times. After 48 h of immersion, a slight change was observed in the diameter (resistance) and the height (capacity) of the half-loop. The loops correspond to the phenomenon of charge transfer, which confirms the aggressive effect of chloride ions [38]. The simulation of the experimental data with the ZSimp software makes it possible to determine the equivalent electrical circuit. The latter provides several characteristic parameters of the system.

The proposed circuit for bare steel includes 3 elements (Fig. 13B), of which R_s represents the resistance of the solution and Q_{cd} a constant phase element (CPE) which represents the capacity of the double layer. The value of the capacitance associated with the capacitive loop of the impedance diagram can be estimated from the relation $C = 1/2\pi fR$ (after converting the CPE into capacitance using the Brug formula); where f corresponds to the characteristic frequency (determined at the maximum of the real part of the loop) and R is the diameter of the loop.

The charge transfer resistance is represented by R_{ct}. The circuit becomes more complex by the application of the polymeric coating (5 elements), with L_p and R_p the inductance and the resistance of the coating respectively. The parameter L_p gives the inductive aspect to the impedance loop. After 24 h of immersion, these last two are replaced by W, a short-circuit term of Warburg, which represents the diffusion.

Table 5 shows the evolution of the characteristic parameters of the PDPA/Steel system during immersion. Following the variation of the characteristic parameters numerous conclusions can be drawn. The charge transfer resistance (R_{ct}) and Warburg coefficient (W) vary with time, providing the suggestion that after an inductive period (t < 24 h), the formation of active centers occurs contributing to perceptible diffusion limitations [71]. However, the capacity of the double layer (Q_{cd}) increases. After 144 h, Q_{cd} increases to $1.403\ 10^{-3}\ S.s^{0.5}$. On the other hand, the resistance of the solution (R_s) remains approximately constant (34–36 Ω). Briefly, the decrease in Q_{cd} and W and the increase in R_{ct}

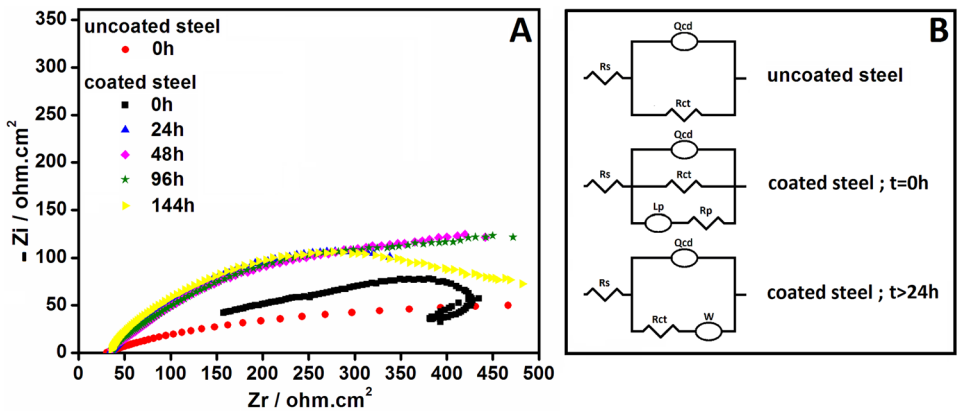

Fig. 13 Electrochemical impedance loops (Nyquist diagram) of PDPA-coated electrode measured at different immersion times in 3% NaCl (**A**). Equivalent electrical circuit (**B**)

Table 5 Evolution of the characteristic parameters of the equivalent circuit of the PDPA/Steel system during immersion

	24 h	48 h	96 h	144 h
R_s (Ω)	34.651	35.882	36.216	35.219
Q_{cd} (10^{-3} S $s^{0.5}$)	5.727	3.197	2.417	1.403
R_{tc} (Ω)	470.4	576.8	510.1	444.5
W (S s^5)	0.2749	0.06715	0.02525	0.05943

shows that the diffusion of corrosion products and the charge transfer decrease. This confirms the good corrosion protection performance of the polymer.

In general, when metals are in contact with a doped semiconductor or an electronically conducting polymer, an electric field is generated limiting the flow of electrons from the metal to oxidizing species, therefore preventing or reducing corrosion rate [72].

Simpler equivalent circuits have been described in the literature [73–75]. Minh and Quoc [65] divide the impedance spectra into three regions:

(i) High frequency region: characterizes the behaviour of the electrolyte. The resistance of the electrolyte is described by R_e in the equivalent circuit (Fig. 14).
(ii) Medium Frequency Region: Indicates the properties of the polymer film that behaves like a dielectric with a capacitive impedance. The behaviour is simulated by a C_{pm} capacitance parallel to the resistance of the polymer film R_{pm}.
(iii) Low Frequency Region: represents the polymer/substrate interface. C_{dl} and R_{ct} are the double layer capacity and the charge transfer resistance of the interface, respectively.

A physical barrier effect from the polymeric film avoids penetration of corrosive agents to the metallic surface and consequently reduce corrosion at the interface coating/electrode. However, this barrier effect depends basically on the

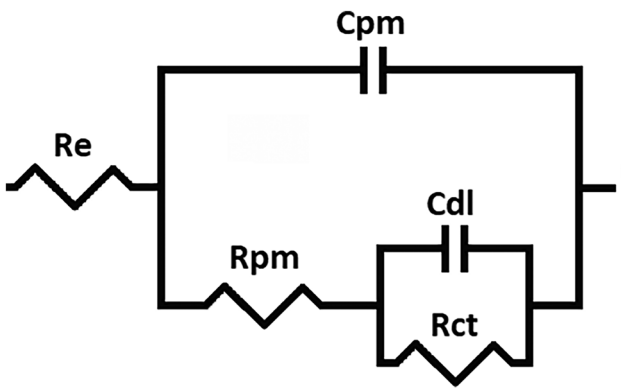

Fig. 14 Equivalent circuit reported in the literature [65]

porosity of the polymeric layer. Instead, chloride (Cl^-) diffusion occurs through ion exchange in the polymer and could be important in the case of doped films [76]. Furthermore, when the anion is released during the reduction of the coating, an anion-exchange process takes place and the polymer is doped by small anions. By this process, chlorides can reach the metal surface [72]. For these reasons, the perfect coating must offer an impermeable obstacle and display durable stability.

Permeability and barrier property are two sides of the same coin; thus the same factors direct both the processes. Different concepts have been explaining the permeable nature of polymers [77]. According to these theories, permeation includes three stages: sorption of molecules in the polymer; diffusion of these molecules from higher concentration/pressure side to lower one and desorption of the molecules from the other side of the film. Mathematically it is defined as: $P = D * S$, where P, D and S are coefficients of permeability, diffusivity and solubility of penetrant in the polymer respectively [77]. The diffusion governs the gaseous permeation, while solubility dominates in water permeation. Generally, permeability depends on several factors such as the nature of the polymer and its thickness, size and shape penetrant, pressure and temperature.

The porosity can be calculating by: $P = \frac{R_1}{R_2} * 10^{-\frac{|\Delta E_{corr}|}{b_a}}$, where P is the total porosity, R_1 and R_2 the polarization resistance of uncoated and coated electrodes respectively, E_{corr} the corrosion potentials and b_a is the anodic Tafel slope for the substrate [78]. The use of this equation needs to adopt that the metal dissolves actively, though the coating is completely stable. In these conditions, the ratio between the anodic current of the coated substrate and that of the uncoated is approximately equal to the porosity of the polymer [78]. Some secondary processes possibly will interfere with the measurement, for example some products may be deposited in the pore.

In general, no chemical bonds exist between the substrate and the polymer. The polymer coating remains at the surface due to the Van der Waals forces between the substrate and the polymer. Ions enter the film if their Van der Waals and ion–dipole interactions with the polymer are large. When the polymer is hydrophobic and the solvent is hydrophilic the interaction energies between the polymer segments and between the solvent molecules are higher than those between the polymer segments and the solvent molecules. In this case, the polymer segments are not solved by the solvent molecules. If the neutral polymer contains polar groups, water molecules will enter the polymer and the polymer phase will eventually contain substantial amounts of water. The situation is different when the polymer is charged, the interface is not permeable and the polymer film behaves like an ion-exchange membrane [71].

Conclusion

Polydiphenylamine has been successfully elaborated on the surface of steel electrodes. A systematic study was carried out using various electrochemical techniques to improve the quality of the formed coating. In this context, the galvanostatic mode has proved to be the most suited to produce homogeneous and highly adherent films. Afterwards, elementary and vibrational analyses by XPS and FTIR confirmed that the synthesized polymer on oxidizable metals has the same chemical compositions and structural characteristics as those usually obtained on noble electrodes. Hence, it was further tested as protective coatings against the dissolution of steel. Analysis by open-circuit potential technique, linear polarization and electrochemical impedance spectroscopy over the immersion time in 3% NaCl solution revealed the stability of the polymeric coating. The initial potential of the covered metallic substrate was shifted to more anodic values compared to the uncoated electrode and a slight decrease of the corrosion current density was recorded during the immersion. The inhibitory efficiency increased from 64.6% at the beginning of immersion to 95.5% after 24 h and reached 97.2% at the end of the test. These results were expected assuming the results of the adherence tests. The interesting electrochemical behavior of PDPA films in aggressive solutions can allow its use in various industries as a protective coating not only for steel but also for other metals such as aluminum, copper and zinc. Studies in the case of these types of metallic substrates are in progress.

Funding This work was supported by the MESRSFC and CNRST (Morocco) under grant No. PPR/30/2015.

Declarations

Conflict of interests The authors declare that they have no known competing financial interests or personal relationships that could have appeared to influence the work reported in this paper.

References

1. Aouzal Z et al (2020) Improvement of the anticorrosion resistance of nickel by polypyrrole coating electrosynthesized in salicylate medium. Mater Today Proc 31:S89–S95. https://doi.org/10.1016/j.matpr.2020.06.237
2. Jadi SB et al (2020) Electropolymerization and corrosion resistance of polypyrrole on nickel bipolar plate for PEM fuel cell application. Mater Today Proc 22:52–56. https://doi.org/10.1016/j.matpr.2019.08.072
3. El Jaouhari A et al (2017) Corrosion resistance and antibacterial activity of electrosynthesized polypyrrole. Synth Met 226:15–24. https://doi.org/10.1016/j.synthmet.2017.01.008
4. El Jaouhari A et al (2018) Comparison study between corrosion protection of polypyrrole synthesized on stainless steel from phthalate and saccharinate aqueous medium. Polym Test 67:302–308. https://doi.org/10.1016/j.polymertesting.2018.03.022
5. González MB, Saidman SB (2015) Electrodeposition of bilayered polypyrrole on 316 L stainless steel for corrosion prevention. Prog Org Coatings 78:21–27. https://doi.org/10.1016/J.PORGCOAT.2014.10.012
6. Nautiyal A, Qiao M, Cook JE, Zhang X, Huang TS (2018) High performance polypyrrole coating for corrosion protection and biocidal applications. Appl Surf Sci 427:922–930. https://doi.org/10.1016/J.APSUSC.2017.08.093
7. Yin Y, Prabhakar M, Ebbinghaus P, Corrêa da Silva C, Rohwerder M (2022) Neutral inhibitor molecules entrapped into polypyrrole network for corrosion protection. Chem Eng J 440:135739. https://doi.org/10.1016/J.CEJ.2022.135739
8. Mehandzhiyski Y, Zhao X, Liu X, Fan B, Zheng X (2022) Optimized Anticorrosion of Polypyrrole Coating by Inverted-Electrode Strategy: Experimental and Molecular Dynamics Investigations. mdpi.com. https://doi.org/10.3390/polym14071356
9. Feliú S, Emelyanenko A, Zhu H, Liu X, Hao H, Zheng X (2022) Influence of Surface Pretreatments on the Anticorrosion of Polypyrrole Electro-Polymerized Coatings for Copper in Artificial Seawater. mdpi.com. https://doi.org/10.3390/met12030383
10. Sang Y et al (2022) Synthetic polyaniline-boron nitride-aqueous epoxy resin composite coating for improving the corrosion resistance of hot-dip galvanized steel plates. Appl Surf Sci 592:153229. https://doi.org/10.1016/J.APSUSC.2022.153229
11. Pan W, Dong J, Gui T, Liu R, Liu X, Luo J (2022) Fabrication of dual anti-corrosive polyaniline microcapsules via Pickering emulsion for active corrosion protection of steel. Soft Matter 18(14):2829–2841. https://doi.org/10.1039/D2SM00062H
12. Wu K, Gui T, Dong J, Luo J, Liu R (2022) Synthesis of robust polyaniline microcapsules via UV-initiated emulsion polymerization for self-healing and anti-corrosion coating. Prog Org Coatings 162:106592. https://doi.org/10.1016/J.PORGCOAT.2021.106592
13. Fuseini M, Mahmoud M, Zaghloul Y, Elkady MF, El-Shazly AH (2022) Evaluation of synthesized polyaniline nanofibres as corrosion protection film coating on copper substrate by electrophoretic deposition. J Mater Sci 57(10):6085–6101. https://doi.org/10.1007/S10853-022-06994-3
14. Wang Q (2022) Preparation of Polyaniline/Epoxy Composite and Its Anti-Corrosion Performance. Int J Electrochem Sci 17:220416. https://doi.org/10.20964/2022.04.26
15. Li X, Liu X, Liu H, Liu X, He R, Meng S (2022) Structure, morphology and anti-corrosion performance of polyaniline modified molybdenum sulfide/epoxy composite coating. Colloids Surf A Physicochem Eng Asp 639:128345. https://doi.org/10.1016/J.COLSURFA.2022.128345
16. Bouabdallaoui M et al (2020) Influence of polythiophene overoxidation on its physicochemical properties and corrosion protection performances. Mater Today Proc 31:S69–S74. https://doi.org/10.1016/j.matpr.2020.06.067
17. Conde-Nicho J, Nicho ME, Rodríguez JA, León-Silva U, Rodríguez-Lelis JM (2022) Corrosion protection by poly(3-hexylthiophene)/poly(methyl-methacrylate) coating of cracked 410 stainless steel. Anti-Corrosion Methods Mater. https://doi.org/10.1108/ACMM-07-2021-2507 (ahead-of-print)
18. Xavier JR (2021) Corrosion protection performance and interfacial interactions of polythiophene/silanes/MnO2 nanocomposite coatings on magnesium alloy in marine environment. Int J Polym Anal Charact 26(4):309–329. https://doi.org/10.1080/1023666X.2021.1887627
19. Yadav PK, Prakash O, Ray B, Maiti P (2021) Functionalized polythiophene for corrosion inhibition and photovoltaic application. J Appl Polym Sci 138(44):51306. https://doi.org/10.1002/APP.51306

20. Zhao Y, Chen M, Liu X, Xu T, Liu W (2005) Electrochemical synthesis of polydiphenylamine nanofibrils through AAO template. Mater Chem Phys 91:518–523. https://doi.org/10.1016/j.matchemphys.2004.12.019
21. Athawale AA, Deore BA, Chabukswar VV (1999) Studies on poly(diphenylamine) synthesized electrochemically in nonaqueous media. Mater Chem Phys 58:94–100. https://doi.org/10.1016/S0254-0584(98)00258-2
22. Bitew Z, Kassa A, Misgan B (2022) Poly(diphenylamine-4-sulfonic acid) modified glassy carbon electrode for voltammetric determination of gallic acid in honey and peanut samples. Arab J Chem 15:103853. https://doi.org/10.1016/J.ARABJC.2022.103853
23. Obrezkov FA, Shestakov AF, Vasil'ev SG, Stevenson KJ, Troshin PA (2021) Polydiphenylamine as a promising high-energy cathode material for dual-ion batteries. J Mater Chem A 9(5):2864–2871. https://doi.org/10.1039/D0TA09427G
24. Ozkan SZ et al (2021) One-step synthesis, characterization and properties of novel hybrid electromagnetic nanomaterials based on polydiphenylamine and Co–Fe particles in the absence and presence of single-walled carbon nanotubes. RSC Adv 11(40):24772–24786. https://doi.org/10.1039/D1RA03114G
25. Khatoon H, Ahmad S (2019) Vanadium Pentoxide-Enwrapped Polydiphenylamine/Polyurethane Nanocomposite: High-Performance Anticorrosive Coating. ACS Appl Mater Interfaces 11(2):2374–2385. https://doi.org/10.1021/ACSAMI.8B17861/SUPPL_FILE/AM8B17861_SI_001.PDF
26. Lingam R (2019) Synthesis and Electrochemical Characterisation of Novel Hybrid Copper/Poly (diphenylamine) (PDPA) Nanocomposites. Int J Recent Technol Eng 8:2277–3878. https://doi.org/10.35940/ijrte.D1156.1284S219
27. Hu J-Q, Yang SZ, Zhang JJ, Guo L, Xu X (2019) Synthesis and Anti-Oxidative Properties of Poly(diphenylamine) Derivative as Lubricant Antioxidant. Pet Chem 59(9):1037–1042. https://doi.org/10.1134/S0965544119090081
28. Muthusankar E, Lee SC, Ragupathy D (2019) Enhanced Electron Transfer Characteristics of Surfactant Wrapped SnO 2 Nanorods Impregnated Poly(diphenylamine) Matrix. Sens Lett 16(12):911–917. https://doi.org/10.1166/SL.2018.4031
29. Bazzaoui M, Bazzaoui EA, Martins JI, Martins L (2004) Electrochemical Synthesis of Polythiophene Coatings on Zinc and a Zinc Alloy in Organic Media. Mater Sci Forum 455–456:484–488. https://doi.org/10.4028/www.scientific.net/MSF.455-456.484
30. Petitjean J, Aeiyach S, Ferreira CA, Lacaze PC, Takenouti H (1995) A new oscillatory electrocheical phenomenon observed in the electropolymerization of pyrrole in MeCN+N(Bu)4PF6 on an Iron electrode studied by the ring-disk-electrode technique. J Electrochem Soc 142(1):136–142
31. Ferreira CA, Aeiyach S, Delamar M, Lacaze PC (1990) Electropolymerization of pyrrole on iron electrodes Influence of solvent and electrolyte on the nature of the deposits. J Electroanal Chem 284:351–369. https://doi.org/10.1016/j.jelechem.2005.02.001
32. Tourillon G, Garnier F (1984) Morphology of conducting organic polymers: Polythiophene and poly(3-methyl thiophene). J Polym Sci 22:33–39. https://doi.org/10.1002/pol.1984.180220103
33. Tourillon G, Garnier F (1983) Stability of Conducting Polythiophene and Derivatives. J Electrochem Soc 130(10):2042–2044. https://doi.org/10.1149/1.2119517
34. Aeiyach S, Bazzaoui EA, Lacaze PC (1997) Electropolymerization of thiophene on oxidizable metals in organic media. J Electroanal Chem 434:153–162. https://doi.org/10.1016/S0022-0728(97)00044-2
35. Odziemkowski M, Krell M, Irish DE (1992) A Raman Microprobe In Situ and Ex Situ Study of Film Formation at Lithium/Organic Electrolyte Interfaces. J Electrochem Soc 139(11):3052–3063. https://doi.org/10.1149/1.2069032
36. Chan HSO, Ng SC, Sim WS, Tan KL, Tan BTG (1992) Preparation and Characterization of Electrically Conducting Copolymers of Aniline and Anthranilic Acid: Evidence for Self-Doping by X-ray Photoelectron Spectroscopy. Macromolecules 25:6029–6034. https://doi.org/10.1021/ma00048a026
37. Golczak S, Kanciurzewska A, Fahlman M, Langer K, Langer JJ (2008) Comparative XPS surface study of polyaniline thin films. Solid State Ionics 179:2234–2239. https://doi.org/10.1016/j.ssi.2008.08.004
38. Chang C-F, Chen W-C, Wen T-C, Gopalan A (2002) Electrochemical and Spectroelectrochemical Studies on Copolymerization of Diphenylamine with 2,5-Diaminobenzenesulfonic Acid. J Electrochem Soc 149(8):E298–E305. https://doi.org/10.1149/1.1491984
39. Kilmartin PA, Wright GA (1997) Photoelectrochemical and spectroscopic studies of sulfonated polyanilines Part I. Copolymers of orthanilic acid and aniline. Synth Met 88:153–162. https://doi.org/10.1016/S0379-6779(97)03854-X
40. Wu M-S, Wen T-C, Gopalan A (2001) Electrochemical Copolymerization of Diphenylamine and Anthranilic Acid with Various Feed Ratios. J Electrochem Soc 148(5):D65–D73. https://doi.org/10.1149/1.1366625
41. Bouabdallaoui M et al (2017) X-ray photoelectron and in situ and ex situ resonance Raman spectroscopic investigations of polythiophene overoxidation. J Solid State Electrochem 21(12):3519–3532. https://doi.org/10.1007/s10008-017-3698-9
42. Eshkenazi V, Peled E, Burstein L, Golodnitsky D (2004) XPS analysis of the SEI formed on carbonaceous materials. Solid State Ion 170:83–91. https://doi.org/10.1016/S0167-2738(03)00107-3
43. Ugalde L, Bernede JC, Del Valle MA, Díaz FR, Leray P (2002) SEM study of the growth of electrochemically obtained polythiophene thin films: Effect of electrolyte and monomer concentration in acetonitrile. J Appl Polym Sci 84:1799–1809. https://doi.org/10.1002/app.10291
44. Abraham KM, Goldman JL, Natwig DL (1982) Characterization of Ether Electrolytes for Rechargeable Lithium Cells. J Electrochem Soc 129(11):2404–2409. https://doi.org/10.1149/1.2123556
45. Shifler DA, Moran PJ, Kruger J (1991) The passivity of iron and carbon steel in anhydrous propylene carbonate solutions. Corros Sci 32(5/6):475–496. https://doi.org/10.1016/0010-938X(91)90102-U
46. Nelson AJ, Glenis S, Frank AJ (1987) XPS and UPS investigation of PF6 doped and undoped poly 3methyl thiophene. J Chern Phys 87(8):5002–5006. https://doi.org/10.1063/1.452815
47. Cai M, Liang Y, Zhou F, Liu W (2011) Tribological Properties of Novel Imidazolium Ionic Liquids Bearing Benzotriazole Group as the Antiwear/Anticorrosion Additive in Poly(ethylene glycol) and Polyurea Grease for Steel/Steel Contacts. ACS Appl Mater Interfaces 3:4580–4592
48. Bazzaoui EA, Bazzaoui M, Aubard J, Lomas JS, Félidj N, Lévi G (2001) Surface-enhanced Raman scattering study of polyalkylthiophenes on gold electrodes and in silver colloids. Synth Met 123:299–309. https://doi.org/10.1016/S0379-6779(01)00299-5
49. Bazzaoui EA, Lévi G, Aeiyach S, Aubard J, Marsault JP, Lacaze PC (1995) SERS spectra of polythiophene in doped and undoped states. J Phys Chem 99:6628–6634. https://doi.org/10.1021/j100017a052
50. Bazzaoui EA, Marsault JP, Aeiyach S, Lacaze PC (1994) Resonance Raman study of polythiophene films in the doped and undoped states. Relations between spectral data and physicochemical properties. Synth Met 66:217–224. https://doi.org/10.1016/0379-6779(94)90070-1
51. Bazzaoui EA, Aubard J, Félidj N, Laurent G, Lévi G (2005) Ex situ and in situ SERS analyses of polybithiophene using roughened Ag and Cu electrodes and multilayer SERS-active systems. J Raman Spectrosc 36:817–823. https://doi.org/10.1002/jrs.1368

52. Bazzaoui EA, Aeiyach S, Lacaze PC (1996) Electropolymerization of bithiophene on Pt and Fe electrodes in an aqueous sodium dodecylsulfate (SDS) micellar medium. Synth Met 83:159–165. https://doi.org/10.1016/S0379-6779(97)80070-7
53. Showkat AM, Cao XT, Kim DW, Islam MR, Lim KT (2015) Characterization of poly(diphenylamine)-gold nanocomposites obtained by self-assembly. IOP Conf Ser Mater Sci Eng 77:1–8. https://doi.org/10.1088/1757-899X/77/1/012007
54. Kim SB, Harada K, Yamamoto T (1998) Preparation of poly(diphenylamine-4,4′-diyl) and related random copolymers by organometallic polycondensation. Electrical, electrochemical, and optical properties. Macromolecules 31:988–993. https://doi.org/10.1021/ma971244f
55. Showkat AM, Cao XT, Kim DW, Kim YH, Lim KT (2016) Self-Assembly Directed One-Step Synthesis of Conducting Poly(diphenylamine)/Gold Nanocomposites. Sci Adv Mater 8:318–321. https://doi.org/10.1166/sam.2016.2486
56. Tang J, Jing X, Wang B, Wang F (1988) Infrared spectra of soluble polyaniline. Synth Met 24:231–238. https://doi.org/10.1016/0379-6779(88)90261-5
57. Dong S, Song FY, Li Z (1992) Electrochemical Synthesis and Characterization of polydiphenylamine. Chin J Chem 10(1):10–16. https://doi.org/10.1088/1742-6596/431/1/012003
58. Md Showkat A, Md Showkat KP, Gopalan AI, Kim SH, Choi SH, Sohn SH (2006) Characterization and preparation of new multi-wall carbon nanotube/conducting polymer composites by in situ polymerization. J Appl Polym Sci 101:3721–3729. https://doi.org/10.1002/app.23359
59. Ozkan SZ, Dzidziguri EL, Karpacheva GP, Bondarenko GN (2011) Synthesis, structure, and properties of new Cu/polydiphenylamine metallopolymer nanocomposites. Nanotechnologies Russ 6(11–12):750–756. https://doi.org/10.1134/S1995078011060115
60. Ozkan SZ, Dzidziguri EL, Chernavskii PA, Karpacheva GP, Efimov MN, Bondarenko GN (2013) Metal-polymer nanocomposites based on polydiphenylamine and cobalt nanoparticles. Nanotechnologies Russ 8(7–8):452–460. https://doi.org/10.1134/S1995078013040113
61. Fenelon AM, Breslin CB (2005) The Formation of Polypyrrole at Iron from 1-Butyl-3-methylimidazolium Hexafluorophosphate. J Electrochem Soc 152(1):D6–D11. https://doi.org/10.1149/1.1831211
62. Gambino D et al (1999) Synthesis, Characterization, and Crystal Structure of [ReO(Me4tu)4](PF6)3 (tu = thiourea). Z Anorg Allg Chem 625:813–819
63. Heinze J, Frontana-uribe BA, Ludwigs S (2010) Electrochemistry of Conducting Polymers s Persistent Models and New. Chem Rev 110:4724–4771
64. Kraljić M, Mandić Z, Duić L (2003) Inhibition of steel corrosion by polyaniline coatings. Corros Sci 45(1):181–198. https://doi.org/10.1016/S0010-938X(02)00083-5
65. Minh L, Quoc V (2013) Layers of Inhibitor Anion – Doped Polypyrrole for Corrosion Protection of Mild Steel. Materials Science - Advanced Topics. InTech
66. Roberge PR, Pierre R (1999) Handbook of Corrosion Engineering. McGraw-Hill
67. Sathiyanarayanan S, Muthukrishnan S, Venkatachari G (2006) Synthesis and anticorrosion properties of polydiphenylamine blended vinyl coatings. Synth Met 156:1208–1212. https://doi.org/10.1016/j.synthmet.2006.08.008
68. Beck F, Barsch U, Michaelis R (1993) Corrosion of conducting polymers in aqueous media. J Electroanal Chem 351(1–2):169–184. https://doi.org/10.1016/0022-0728(93)80232-7
69. Christensen PA, Hamnett A (1991) In situ spectroscopic investigations of the growth, electrochemical cycling and overoxidation of polypyrrole in aqueous solution. Electrochim Acta 36(8):1263–1286. https://doi.org/10.1016/0013-4686(91)80005-S
70. Hien NTL, Garcia B, Pailleret A, Deslouis C (2005) Role of doping ions in the corrosion protection of iron by polypyrrole films. Electrochim Acta 50(7–8):1747–1755. https://doi.org/10.1016/j.electacta.2004.10.072
71. Inzelt G (2018) Conducting polymers: past, present, future. J Electrochem Sci Eng 8(1):3–37. https://doi.org/10.5599/jese.448
72. Deshpande PP, Jadhav NG, Gelling VJ, Sazou D (2014) Conducting polymers for corrosion protection : a review. J Coat Technol Res. https://doi.org/10.1007/s11998-014-9586-7
73. Paliwoda-Porebska G, Rohwerder M, Stratmann M, Rammelt U, Duc LM, Plieth W (2006) Release mechanism of electrodeposited polypyrrole doped with corrosion inhibitor anions. J Solid State Electrochem 10(9):730–736. https://doi.org/10.1007/s10008-006-0118-y
74. Plieth W, Bund A, Rammelt U, Neudeck S, Duc LM (2006) The role of ion and solvent transport during the redox process of conducting polymers. Electrochim Acta 51(11):2366–2372. https://doi.org/10.1016/j.electacta.2005.03.087
75. Rammelt U, Duc LM, Plieth W (2005) Improvement of protection performance of polypyrrole by dopant anions. J Appl Electrochem 35(12):1225–1230. https://doi.org/10.1007/s10800-005-9033-7
76. Shinde VP (2017) Study of water transport characteristics of poly (o -ethylaniline) coatings : corrosion mechanism. Ionics. https://doi.org/10.1007/s11581-017-2213-8
77. Sangaj NS, Malshe VC (2004) Permeability of polymers in protective organic coatings. Prog Org Coatings 50(1):28–39. https://doi.org/10.1016/j.porgcoat.2003.09.015
78. Herrasti P, del Rio AI, Recio J (2007) Electrodeposition of homogeneous and adherent polypyrrole on copper for corrosion protection. Electrochim Acta 52:6496–6501. https://doi.org/10.1016/j.electacta.2007.04.074